Development of an Experimental Procedure to Quantify Dynamic Factors of Spur Gears

UNDERGRADUATE HONORS THESIS

Presented in Partial Fulfillment of the Requirements for Graduation with Honor's Research Distinction in the Department of Mechanical and Aerospace Engineering at The Ohio State University

By

Thomas Gullo

Undergraduate Program in Mechanical Engineering

The Ohio State University | 2018

Thesis Committee:

Dr. Ahmet Kahraman

Dr. David Talbot

Abstract

Evaluation of bending fatigue failures has traditionally been done experimentally where spur gear specimens are run under different levels of torque to generate stress-life curves for gear designers to use. As life expectancy of any transmission is typically very long, these stress-life curves may also be extended to cover long cycle regimes. As such, collection of gear fatigue data requires significant amount of test time. One way of reducing data collection time is to operate the gears at higher speeds to increase loading frequency. This often results in dynamic effects, which increases tooth loads and dynamic root stresses in the process altering stress-life curves. The dynamic factor (*DF*), defined as the ratio of the peak values of stress under dynamic and static conditions, must be quantified in order to account for such dynamic effects. In this study, an experimental set-up is developed to measure root fillet strains of a spur gear under both low-speed (quasi-static) and high-speed (dynamic) conditions. A strain-gaged spur gear is loaded in a three-shaft arrangement, and resultant root strains are measured and transferred to a data analysis system. The ratio of the peak values of the stress signal under dynamic and static conditions are computed as the stress-based dynamic factor of the gear pair under these operating conditions. As the gaged gear is operated in an idler arrangement, sets of *DF* values are established at different levels of torque transmitted.

Dedication

To my family and friends.

Acknowledgements

I would like to extend my thanks to Dr. Kahraman for his extensive help and involvement throughout the formulation of this work. I would also like to thank Isaac Hong for his guidance and willingness to help with the experimentation, as well as Dr. Talbot for serving on my defense committee. Thank you to Jonny Harianto for the support as well as all the staff and students involved in the Gear and Power Transmission Laboratory for any support along the way, and thank you to the Gear and Power Transmission Laboratory Consortium members for the support and ultimately enabling me to pursue this undergraduate research. Thank you to the College of Engineering for granting me a scholarship to complete an undergraduate thesis. Finally, I would like to thank my family and friends who supported me each and every day.

Vita

1995……...……Born in Hartford, Connecticut

May 2014…….Olentangy Liberty High School

Powell, Ohio

August 2017 to Present…….……. Research Associate, GearLab

Fields of Study

Major Field: Mechanical Engineering

Table of Contents

List of Tables

List of Figures

Chapter 1

Introduction

1.1 Background and Motivation

Gears are the primary components used in power transmission systems in automotive, aerospace, and other industrial applications. Based on duty cycles in a given application, each gear must be designed such that the life expectancy requirement can be met. In order to determine the life of a gear component, one must know not only the type and amount of load that the gear must carry, but also the stresses that it experiences under such loads. The gear analysis tools available can be used to predict gear stresses under static conditions. However, gears are operated at elevated speeds where dynamic forces are often larger than their static counterparts, resulting in dynamic stresses that are higher than static ones. As such, predicted static stresses $\sigma_s(t)$ must be corrected to account for any dynamic effects. An accurate estimation of the design life of a gear is heavily dependent on accurate knowledge of the dynamic stresses.

Figure 1.1 provides a comparison of a quasi-static root strain time history $\sigma_s(t)$ measured at a very low rotational speed when the dynamic effects are negligible and its dynamic counterpart $\sigma_d(t)$ at a given higher rotational speed value [1]. It is evident here

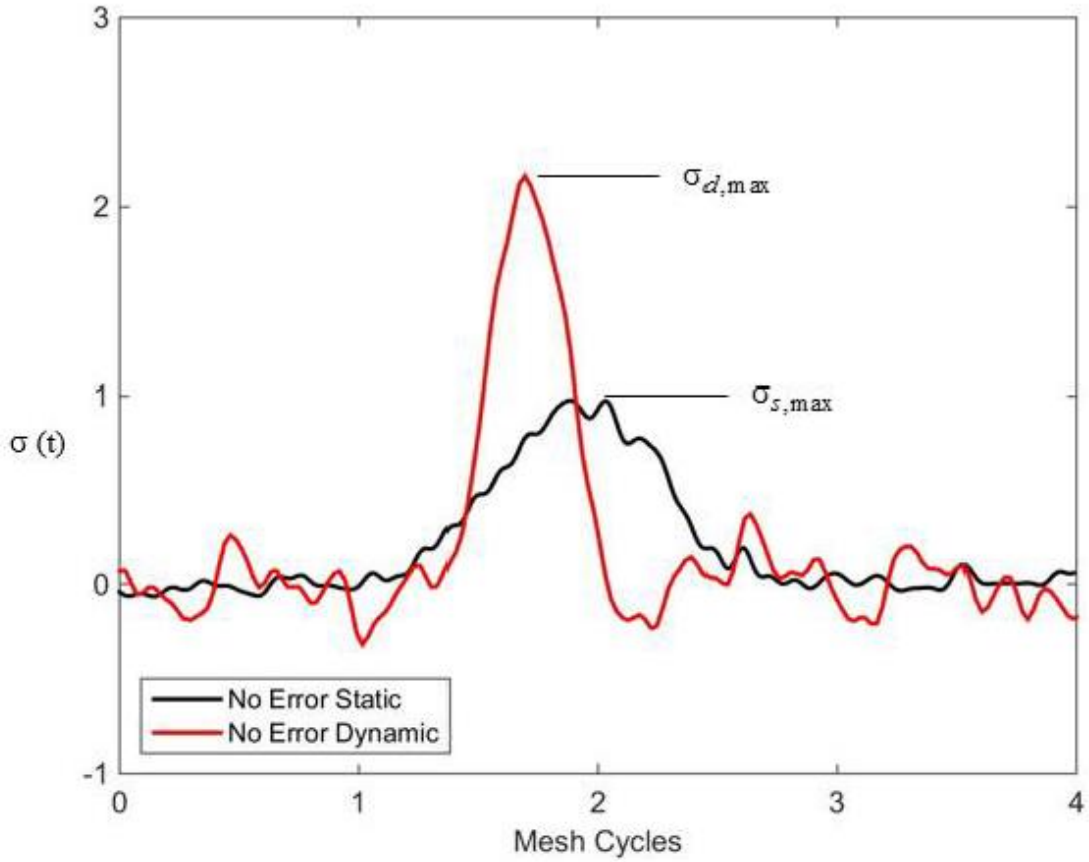

Figure 1.1: Demonstration of dynamic effects on root strain of a spur gear [1].

that these two signals differ significantly with the maximum value of $\sigma_d(t)$ being nearly two times higher than the maximum value of $\sigma_s(t)$. Using these maximum values of the two signals, a dynamic magnification parameter, or *DF*, can be defined as

$$DF = \frac{\sigma_{d,\max}}{\sigma_{s,\max}}. \tag{1.1}$$

This formulation quantifies the difference in dynamic stress and quasi-static stress by forming a scalar that, when multiplied to static stress, represents dynamic stress. Ultimately, the *DF* value established at a given rotational speed can be used to scale fatigue data properly.

As dynamic contact mechanics models are not reliable to predict *DF*, partly because the type of machine and test gear design influence the dynamic response, it must be determined experimentally. This undergraduate study proposes a methodology for experimental evaluation of *DF*.

1.2 Literature Review

The dynamic factor has been studied extensively for years, resulting in it being expressed in multiple fashions. Many of these formulations have been modified since the beginning of gear dynamic studies dating back about a century. Originally, Walker introduced a dynamic factor which was then adapted by Barth as a ratio of static and dynamic loads [2]. A study done by Buckingham furthered the knowledge on dynamically loaded gears through prediction of dynamic effects [3]. Harris developed more accurate ways to measure and quantify dynamic stresses in gear pairs involving photo-elastics [4]. The AGMA (American Gear Manufacturers Association) has even modified their

formulation as recently as 2001. Currently, the AGMA standard defines the dynamic factor in terms of dynamic and static forces by following

$$K_v = \frac{F_d + F_t}{F_t} \tag{1.2}$$

where F_d represents the additional forces on the tooth due to the dynamics of the system and F_t is the transmitted tooth force not accounting for dynamics [5]. With the root stresses of the tooth being linearly proportional to the force it carries, Eq. (1.1) and (1.2) are related as long as the forces in Eq. (1.2) are tooth forces. It is important to note that this formulation not valid within resonant frequencies of the system and its components.

It is critical that the *DF* is known for a gear in any power transmission system within ranges of speed and torque transmitted for proper design of the gear for the application in hand. From a research point of view, this requires a deformable-body model like the recently developed models of Talbot et al [6] and Talbot and Kahraman [7]. These models, if validated, are not only to be used to predict the *DF* based on dynamic root stresses, but also relate it to measured vibratory behavior as attempted experimentally [8] and theoretically [9]. This points to the necessity of collecting repeatable and noise-free root stress data from a high-speed gear so that the *DF* can be quantified.

As the instrumented gear rotates the signal must be processed by a stationary data collection and analysis system, strain signals must be transferred from rotating shafts to the stationary frame. This can be done in two ways. One uses a telemetry system placed on rotating gear to transmit strain signals in a wireless manner [10]. This requires expensive,

dedicated instrumentation, and it is undesirable since it adds inertia to the rotating gear, potentially altering the dynamic behavior.

The other way is to use a slip ring attached to the end of the shaft holding the gear to transmit the signals. This has been used in the previous investigations [1, 6, 8] with mixed success since (i) the strain circuit often cannot be balanced on the rotating side, and (ii) lateral and axial shaft vibrations introduce sizable noise to the signal transmitted by the slip ring. This study aims at exploring ways to overcome such difficulties to improve the *DF* measurement via slip rings.

1.3 Objectives and Scope

The main objectives of this Honors Undergraduate Thesis are as follows:

(i) Develop an experimental methodology for quantifying dynamic root stress factors.

(ii) Implement this methodology on a test gear pair operated in a fatigue test machine.

(iii) Perform low and high-speed measurements of root stresses to quantify dynamic factors of the intended setup.

(iv) Statistically analyze the data to determine the changes in dynamic factor with load, in the process demonstrating the effectiveness of the measurement method developed.

The scope of this work will be limited to determining the dynamic factor of the test conditions implemented with a single research gear pair. The methods used in the Undergraduate Thesis will form the basis of a MS thesis in which measured dynamic factors are compared on a machine developed in the Gear and Power Transmission Research Laboratory as well as an ISO standard machine.

1.4 Outline

Chapter 2 discusses the experimental methods used in order to carry out the required testing of this project. Highlighted topics in this chapter include the introduction of the test machine used, the instrumentation of the test gear, as well as hardware used and the data acquisition techniques implemented. Chapter 3 will present the data acquired from each of the tests completed. Data processing techniques as well as statistical analysis will be detailed in this chapter. Finally, Chapter 4 provides an overview of the study as well as presents conclusions based on the results. Future considerations for a subsequent MS thesis will be presented as well.

Chapter 2

Experimental Set-up

2.1 Introduction

In this chapter, the gear bending fatigue test machine developed as part of another thesis project [11] will be introduced first. A concept of measuring dynamic factors of gears tested in this machine will be introduced. This concept relies on comparing strains in the root fillet region of a test gear measured under both quasi-static (very low-speed operation with no dynamic effects) and desired high-speed conditions. Strain gage placement on the gear teeth will be described. As the gages rotate with the test gears within the gearbox, transfer of their signals to the fixed instrumentation becomes a major task as direct implementation of slip rings on the test gearbox often result in very noisy strain signals. A method of isolating the slip ring to transfer strain signals to the fixed frame with minimal noise will be illustrated. Analysis of strain data under steady-state conditions will be described together with instrumentation used to perform the data acquisition and analysis.

2.2 Machine Set-up

For this study, a test machine set-up that was designed to rotate certain test gears under load at high-speed conditions was used. Figure 2.1 shows an overall view of this test machine that was designed and developed earlier for another study [11] aiming at quantifying tooth bending fatigue lives of spur gears under different loading conditions. This machine uses a "four square" or "back-to-back" configuration. In this configuration, two gearboxes at the same center distance and gear ratio are connected to each other via flexible shafts to form a closed power circulation loop that is loaded manually via a split coupling loading device. The top view image and schematic of gearboxes and their connecting shafts shown in Figure 2.2(a-b) demonstrate this closed loop. The gearbox to the left, called the test gearbox, and the one to the right, called the reaction gearbox, are kinematically identical. They both have three shafts supported by rolling element bearings to transmit torque in an idler configuration. Shafts holding the two outer gears of both gearboxes are connected to each other by long and slender shafts. With a certain amount of torque trapped in the loop through a torque arm and calibrated weights as shown in Figure 2.3, a small 30 HP AC motor connected to one of the outer reaction gearbox shafts overcomes the power losses of the loop to spin it at desired speed values.

Figure 2.4(a) shows a front view of the test gearbox with the front cover removed for demonstration purposes. Three test gears of spur type forming a two-mesh gear train are evident from this figure. Two larger identical gears, both having 25 teeth, form the input and output for this gear train while the smaller 17-tooth gear in the middle assumes

Figure 2.1: Gear bending fatigue test machine used in this study. Safety covers removed for demonstration purposes (Adapted from Hong [11]).

(a)

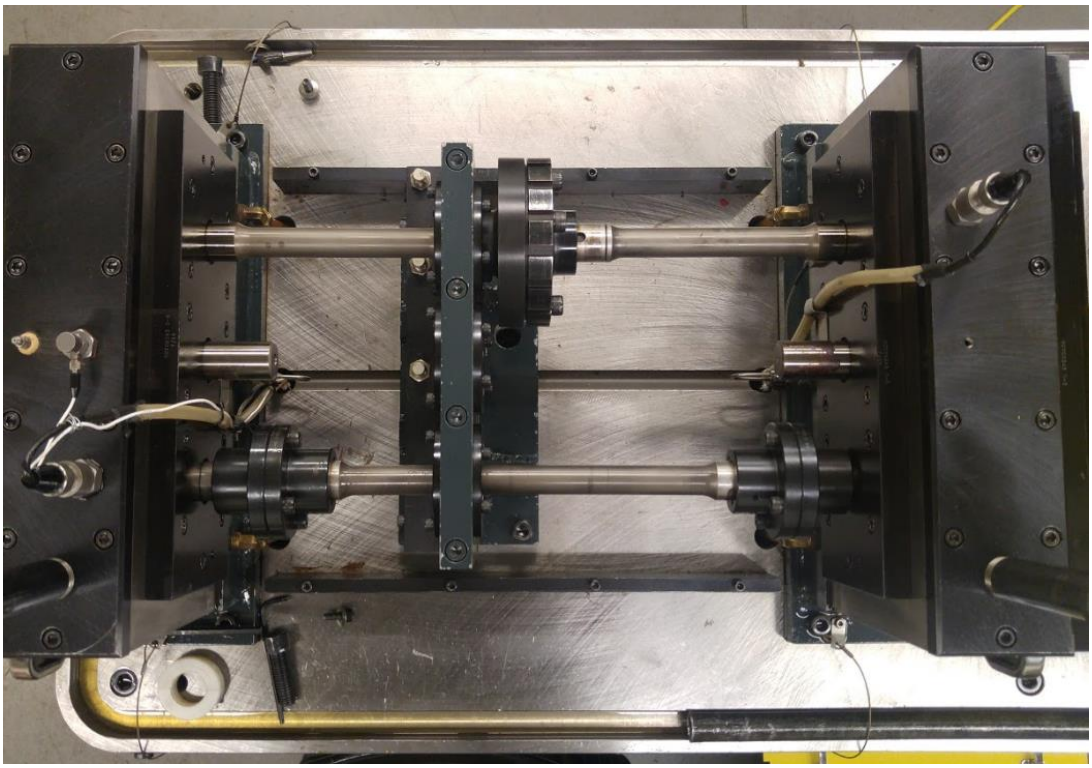

(b)

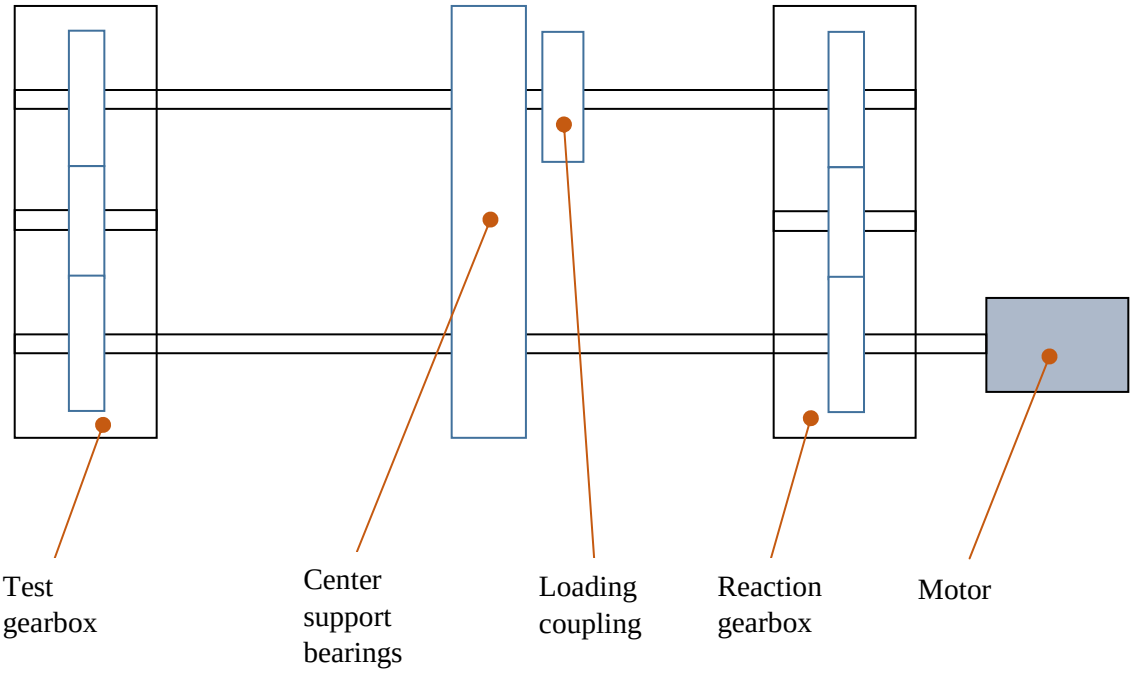

Figure 2.2: (a) Top-view of the test machine showing the closed power circulation loop and (b) a schematic of the same with main components labeled.

Figure 2.3: Application of the torque to the power circulation loop.

the role of an idler gear, similar to the planet gears in an epicyclic gear set [12]. This machine uses a three gear, two mesh set-up for each gearbox. In this idler arrangement, the 17-tooth gear is in contact with both outside gears. As shown in Figure 2.4(b), opposite flanks of a tooth of this gear comes to contact with these two gears as the lines of action of the two meshes are not parallel, but intersect. As such, an arbitrary point A shown in the root fillet of the 17-tooth gear will experience tensile stress as it is contact with one of the side gears and compressive stress as it comes to contact with the other side gear. This condition can be characterized as a fully-reversed loading condition by using fatigue terminology. A schematic of the expected stress at this point A is shown in Figure 2.4(c). As such, a gage placed at this point A will register maximum compressive and tensile stress values that can be compared to those under static conditions to determine dynamic factors.

2.3 Test Gear and Its Instrumentation

The 17-tooth test pinion used in this study was designed by Hong [11] to collect root stress-tooth bending fatigue life data. As seen in Figure 2.4(b) and Figure 2.5(a), it has non-standard proportions. Specifically, its tooth dedendum extends considerably (i.e. the root diameter is much smaller) to have very long teeth whose root stresses are very high in comparison to its contact stresses. Also noted here is that a circular root fillet is adapted so that root stresses are not impacted by any stress concentrations caused by a smaller root fillet radius. This would make the strain gradient along the root fillet very steep, in the process allowing manufacturing and gage placement errors to have significant adverse effect on the measurements. In its full-circle root flank shape, such effects are fully eliminated. As these extended root fillets are obtained through hard gear grinding

(a)

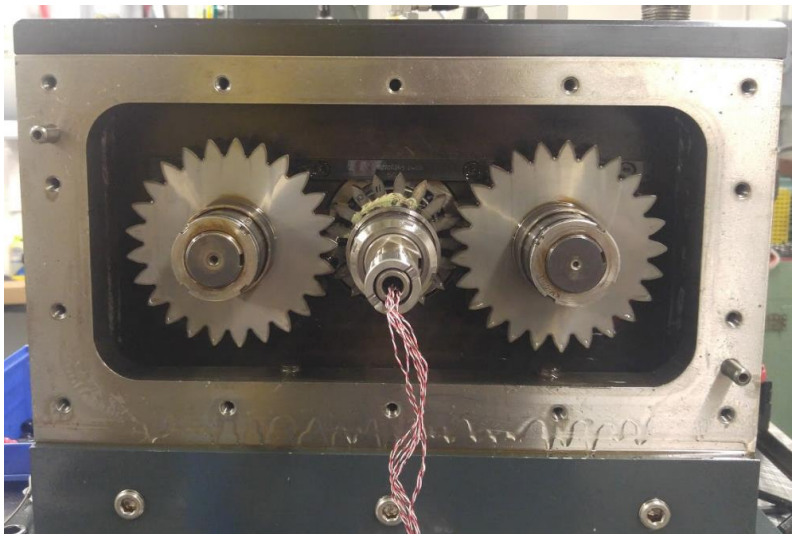

(b)

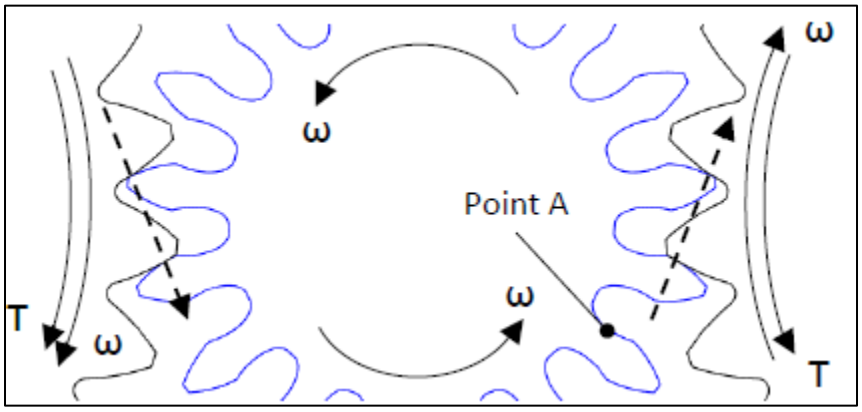

(c)

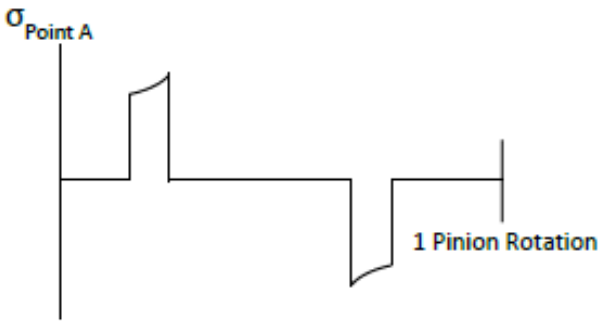

Figure 2.4: (a) A view of the test pinion within the test gearbox, (b) loading of the idler gear by the two side gears, and (c) a resultant stress profile (adapted from Hong [11]).

(a)

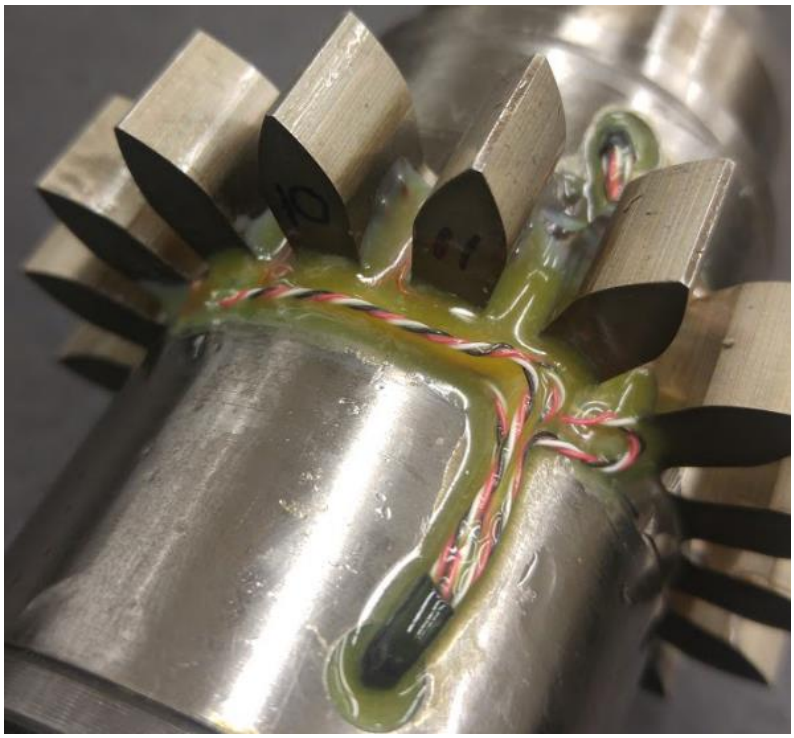

(b)

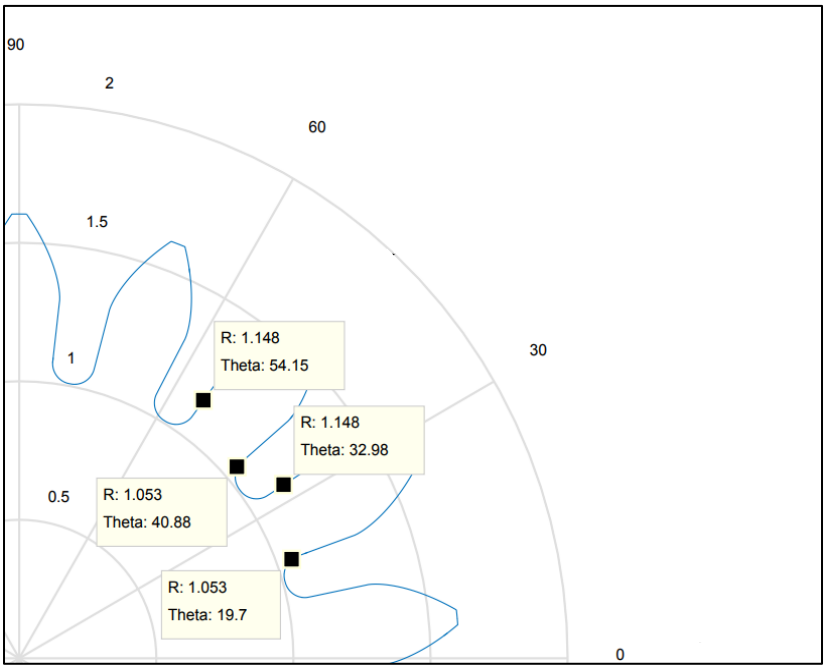

Figure 2.5: (a) Close-up of the gaged test pinion and (b) the schematic of two teeth with gage locations.

procedures, root fillets of all teeth of the pinion have identical shapes such that measuring root stresses at one tooth will be representative of all the teeth of the pinion.

A more detailed description of the 17-tooth test pinion parameters is outlined in Table 2.1. It meshes two identical 25-tooth side gears at a center distance of 91.5 mm. The side gear geometries seen in Figure 2.4(b) are such that their root stresses are significantly lower than that of the pinion. As such, the most likely failure mode in this set-up is the tooth breakage of the pinion due to bending fatigue. Also noted that the gear ratio of 17:25 represents a hunting ratio, meaning that two specific teeth of mating gears will not come to contact frequently such that the contact conditions are randomized.

The 17-tooth pinion was gaged in eight total locations. Four gages were placed in two consecutive teeth as shown in Figure 2.5(b). The other four gages were placed on the teeth opposite to the first two teeth gaged. On each tooth, one gage was placed on the left root fillet at a radius of 29.16 mm (1.148 in) and another on the right root fillet at a radius of 26.75 mm (1.053 in). The left side gages at higher radius are at a lower stress location while the other two are at a relatively higher stress location near the root center.

2.4 Measurement Systems

2.4.1 Strain Measurements

Each of the eight gages was implemented in a quarter-bridge configuration. This configuration is typically used to measure either axial or bending strain. In this study, gages were intended to measure tooth bending strain as they were aligned in the direction of tooth loading. The nominal resistance of each gage was $R_g = 350$ ohms that was confirmed

Table 2.1: Basic parameters of the test pinion [11].

Parameter [unit]	**Value**
Number of Teeth	17
Normal Module [mm]	4.354
Pressure Angle [deg]	26.842
Pitch Diameter [mm]	74.010
Base Diameter [mm]	66.035
Major Diameter [mm]	81.475
Face Width [mm]	12

using a multi-meter. Each gage had gage factor of $GF = 2.06$, which is used by the NI DAQ system to convert the change in voltage from each gage to a strain following

$$\frac{V_o}{V_{EX}} = \frac{R_3}{R_3 + R_g} - \frac{R_2}{R_1 + R_2} \tag{2.1}$$

where V_o is the output voltage, V_{EX} is the excitation voltage, and R_1 to R_3 are resistances of dummy gages completing the quarter bridge. The relation between gage factor and the measured strain is given as

$$\frac{\Delta R_g}{R_g} = GF \frac{\Delta L}{L} = GF\, \varepsilon \tag{2.2}$$

where ΔR_g is the change in gage resistance due to deformations, and $\varepsilon = \frac{\Delta L}{L}$ is the strain experienced by the gage. Finally, the measured bending strain ε is simply converted to bending stress σ by using Hooke's Law as

$$\sigma = E\, \varepsilon \tag{2.3}$$

where E is the modulus of elasticity of the alloy steel gear material.

2.4.2 Slip Ring Implementation

There are alternate ways to transmit an electronic signal from a rotating piece to a stationary data acquisition system (DAQ), ranging from rotary signal transmission devices called slip rings to sophisticated telemetry systems [10]. In this study, the transfer of measured strain signals from the rotating pinion shaft to the DAQ will be done using an end-of-shaft slip ring. This slip ring set-up is shown in Figure 2.6(a) and depicted

schematically in Figure 2.6(b). The test shaft holding the gaged pinion is hollow such that gage wires can be extended to the free end of the shaft that protrudes out of the test gearbox. The wires are then run through an elastomer tube and finally to solder points of the rotating part of the slip ring. Internally, the slip ring has stationary brushes that are in constant contact with a conductive core that is rotating with the shaft. The contact of these brushes on the core transmit separate channels of signals from the rotating hollow test shaft to the stationary portion of the slip ring.

One major issue with end-of-shaft slip rings is that the transmitted signal might have a significant noise content when the slip ring is directly attached to the shaft. In this study, in order to avoid such undesirable noisy signals, an elastomer tube was placed between the structure holding the slip ring and the end of the shaft, in the process isolating the slip ring from the shaft vibrations to improve the signal-to-noise ratio drastically.

2.4.3 Data Acquisition Set-up

A robust system of data collection is needed in order to obtain a sufficient amount of data points to mitigate aliasing effects and increase overall resolution of the measurements. When the side gears in Figure 2.4(a) are rotating at $\Omega_g = 3000$ rpm (speed of pinion: $\Omega_p = \frac{Z_g}{Z_p}\Omega_g = 4412$ rpm where $Z_g = 25$ teeth and $Z_p = 17$ teeth), the gear mesh frequency becomes $f_m = \frac{1}{60}\Omega_g Z_g = \frac{1}{60}\Omega_p Z_p = 1250$ Hz, meaning that a tooth on the test pinion will go through a complete mesh cycle in $(1250)^{-1} = 0.0008\,\text{s}$ (0.8 ms). From previous studies [6, 8], a sample rate that includes more than 30 data points per mesh

(a)

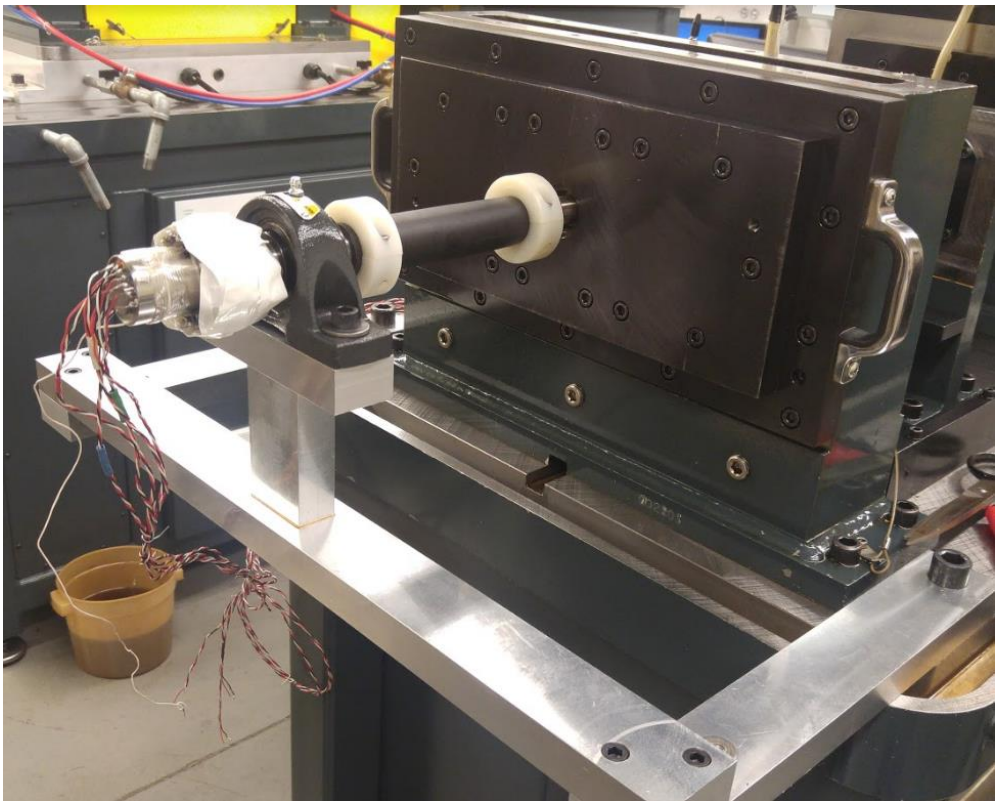

(b)

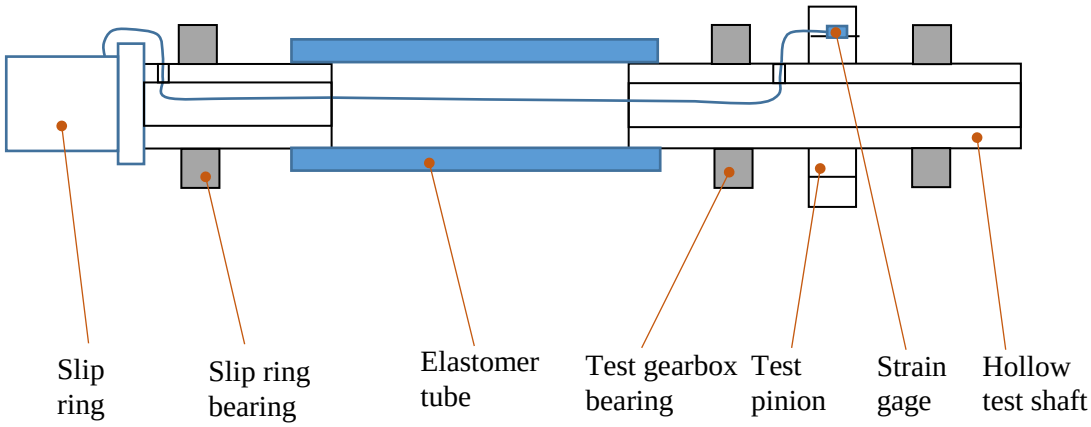

Figure 2.6: (a) Physical slip ring arrangement with (b) a schematic of the slip ring arrangement.

cycle per gage will be sufficient in capturing the peak strain value of a mesh cycle. The NI PXIe 1071 Chassis is used in data collection such that these requirements can be met. With a 100 kHz sampling rate capacity for a maximum of 10 channels, a resolution of approximately 80 points per mesh at $\Omega_g = 3000$ rpm is achieved here.

The strain signal from the slip ring is initially transferred to an NI 4330 Input Module which is attached to the NI PXIe 1071. As the signal is sampled, the NI Max software sends each signal to be processed by LabVIEW running on a PC. This LabVIEW program interacts directly with the NI Max software in which specifications, such as gage factor and gage resistance, for each gage are accepted and utilized in the PXIe 1071 chassis. The physical representation and schematic of the DAQ setup can be found in Figure 2.7(a-b).

From test to test, the LabVIEW program is modified to account for different requirements of the test. For the quasi-static tests at $\Omega_g = 150$ rpm, data collection must be run for a longer period of time compared to the steady-state dynamic tests to capture the same number of gear mesh periods. Due to memory limitations of each outgoing file in LabVIEW, each data segment was limited to 30-seconds long, sampled at a rate of 100 kHz. Quasi-static tests were also run before and after dynamic steady state tests to ensure consistency for a total of three tests per load. A total of three loads are tested, denoted as L, $1.13L$, and $1.33L$, to consider how changes in load affects results.

(a)

(b)

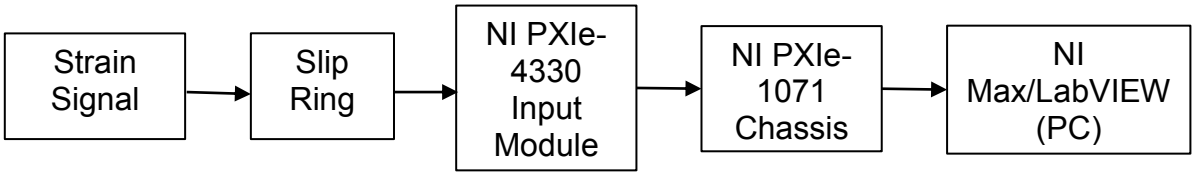

Figure 2.7: (a) Physical data acquisition systems setup and (b) a block diagram representation of the data acquisition.

2.5. Summary

In this chapter, the gear bending fatigue test machine developed as part of another thesis project [11] was introduced. A method of measuring dynamic factors of gears tested in this machine was explained. This method employs tooth root strain gages to compare strains measured under both quasi-static (very low-speed operation with no dynamic effects) and desired high-speed conditions. Strain gage placement on the gear teeth was described. A method of isolating the slip ring to transfer strain signals to the fixed frame with little to no noise was illustrated. Analysis of strain data under both steady-state and low-speed conditions was described together with instrumentation used to perform data acquisition and analysis.

Chapter 3

Experimental Results

3.1 Introduction

This chapter presents and discusses results obtained in the test procedure outlined in Chapter 2. Data analysis details will be described in Section 3.2, and root strain measurements analyzed with this data analysis process will be presented in Section 3.3 for different transmitted torque values at two rotational speeds of $\Omega_g = 150$ rpm (quasi-static condition with negligible dynamic effects) and $\Omega_g = 3000\,\text{rpm}$ (high-speed dynamic fatigue test condition). Dynamic factors will be calculated from acquired data, and will be analyzed statistically to assess their severity and implications will be discussed.

3.2 Data Analysis

The raw strain data for each test run was processed using modified versions of the same MATLAB code. Modifications were in the form of parameterization so that proper inputs for quasi-static and dynamic runs could be accounted for in data processing, such as different mesh frequencies for different speeds. Once data was read in, a low-pass filter of 5000 Hz was applied to the raw strain signal to improve the signal-to-noise ratio. Further, the DC offset was removed from the signal. The filtered data was then parsed for the peak

strains of each mesh cycle in both tensile and compressive sides. These two sets of peak values were analyzed statistically to determine the dynamic factor. Plots of the strain signal as well as histograms representing the relative probability of an occurrence of certain stress levels were plotted as well, and will be detailed in the next section.

3.3 Strain Measurements

As described in Chapter 2, there were multiple torque and speed levels considered in this study. The three torque load levels considered were L, 1.13L and 1.33L with L representing the lowest torque value transmitted. At each load, a quasi-static test at $\Omega_g = 150$ rpm, and a dynamic test at $\Omega_g = 3000$ rpm were performed. The following subsections will separate the data into quasi-static and dynamic test runs and discuss the findings.

3.3.1 Quasi-static Test Results

Plots of the strain time histories were captured and presented at $\Omega_g = 150$ rpm for each load considered. Tensile and compressive peaks of each load cycle were determined and sorted into normalized histograms (probability of occurrence distributions) to show the distribution shape of each test run. If the test gears were to be perfect with no once-per-revolution errors (eccentricities, wobble, and gear runout) and tooth-to-tooth variations (tooth profile errors, surface undulations, tooth spacing, root shape errors, and tooth indexing errors), then one would expect that each tooth entering the gear mesh is loaded the same way such that peak strains measured at a root are constant. Considering a gaged

tooth on the 17-tooth test pinion defined in Table 2.1 meshes with two 25-tooth gears, the gaged tooth comes to contact with different teeth of the mating gears each time since the ratio 17:25 represents a hunting ratio. As such, even very minute errors on mating 25-tooth gears might cause variations to the force carried by the gaged tooth of the 17-tooth pinion. This variation must be assessed and analyzed statistically.

Figure 3.1(a) shows a three rotation long segment of the raw strain signal at the lowest load level *L*. Here, three tensile and compressive peaks are observed with spacing between adjacent tensile and compressive peaks representing nearly ½ rotation of the test pinion as the gaged tooth travels between the two gear meshes shown in Figure 2.4. The raw and filtered versions of the same data in Figure 3.1(a) differ slightly, indicating that noise induced by slip rings are marginal at this low-speed condition. The maximum strains realized in the compressive side on the gage were about 1550 μstrains, whereas maximum strains for the tensile side were hovering around 1450 μstrains. Figure 3.1(b) and (c) show probability distributions of compressive and tensile root stress peaks. These distributions, formed by 1605 data points (representing 1605 revolutions of the pinion), show percentage of occurrences of each stress level using a bin size of $\sigma = 1$ MPa. The average stress was found to be $\sigma = 324.7$ MPa for the compressive peaks and $\sigma = 306.1$ MPa for the tensile peaks.

Segments of the raw and filtered strain signal of the next load level 1.13*L* are shown in Figure 3.2(a). Compressive strain peaks were seen to reach 1900 μstrains, while the peaks are at about 1800 μstrains. The corresponding relative distributions for each of the

(a)

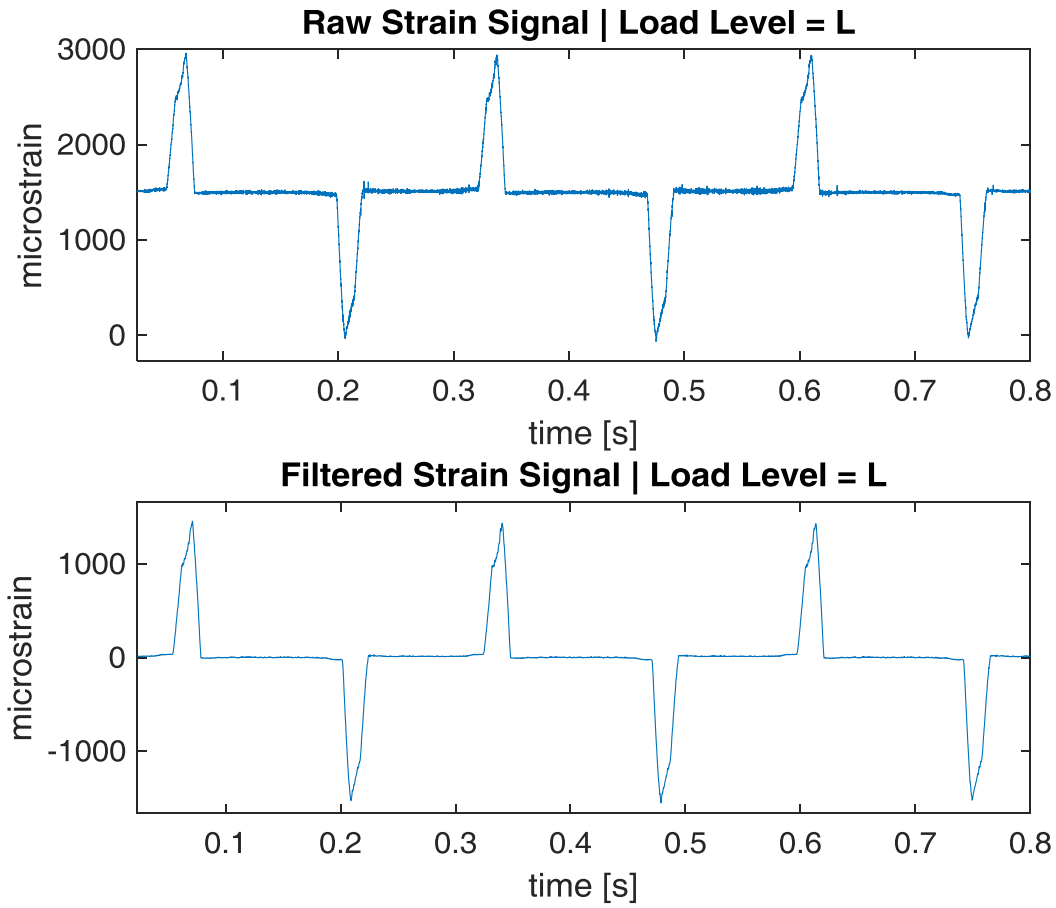

Figure 3.1: (a) Quasi-static strain time history sample for the load level *L*, and (b, c) the accompanying histograms of maximum compressive and tensile stresses.

Figure 3.1: Continued

(b)

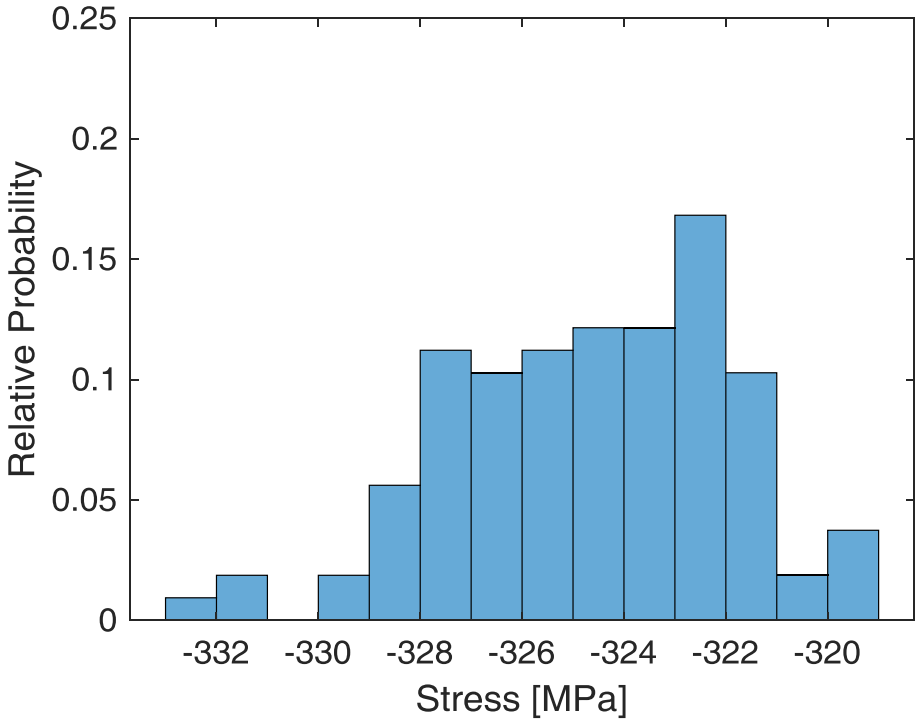

(c)

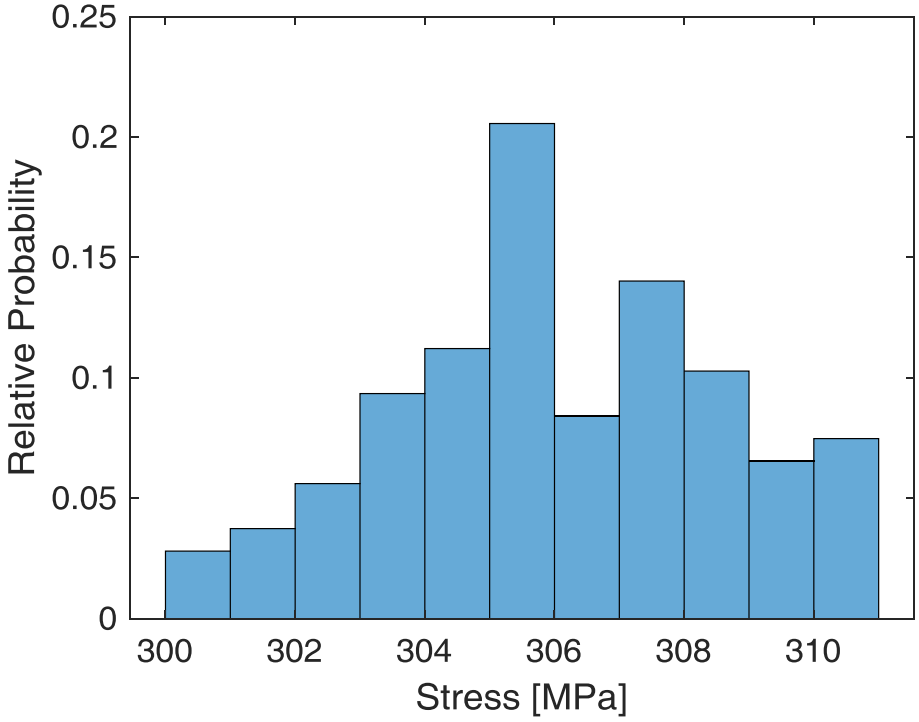

compressive and tensile root stress peaks are shown in Figure 3.2(b, c), again using a bin size of $\sigma = 1$ MPa and 1605 rotations of data. Average root stresses in the gaged pinion tooth were found to be $\sigma = 403.1$ MPa on the compressive side and $\sigma = 376.8$ MPa on the tensile side.

Finally, results for the highest load level of 1.33*L* are presented in Figure 3.3(a) in the same format as two previous figures. Here, peak compressive and tensile strains were nearly 2150 and 2000 μstrains, respectively. Relative probability distributions shown in Figure 3.3(b, c) for 2640 pinion revolutions indicate that the average peak values of compressible and tensile stresses were $\sigma = 434.5$ and 400.2 MPa, respectively.

As one would expect, the root stresses measured at the gage location increase linearly with load. The ratio of average values of the maximum tensile stress for 1.33*L* is 30.7% higher than that of *L* (400.2/306.1=1.307) indicating that a 33% increase in torque transmitted caused about 31% increase in tensile stresses. For the compressive side, peaks the ratio of average peak stresses for the same two load levels is 434.5/324.7=1.338, which is again very close to the load ratio of 1.33.

It can be noted that the stresses due to the compressive loading are consistently higher than the stresses from the tensile loading. This is due to radial forces on the gear tooth. The resultant force in the gear mesh acts perpendicular to the contact surfaces of each tooth. The component radial and tangential forces acting on the gear tooth depend on pressure angle, or the angle the line of action makes with a tangent on the gear base circle.

(a)

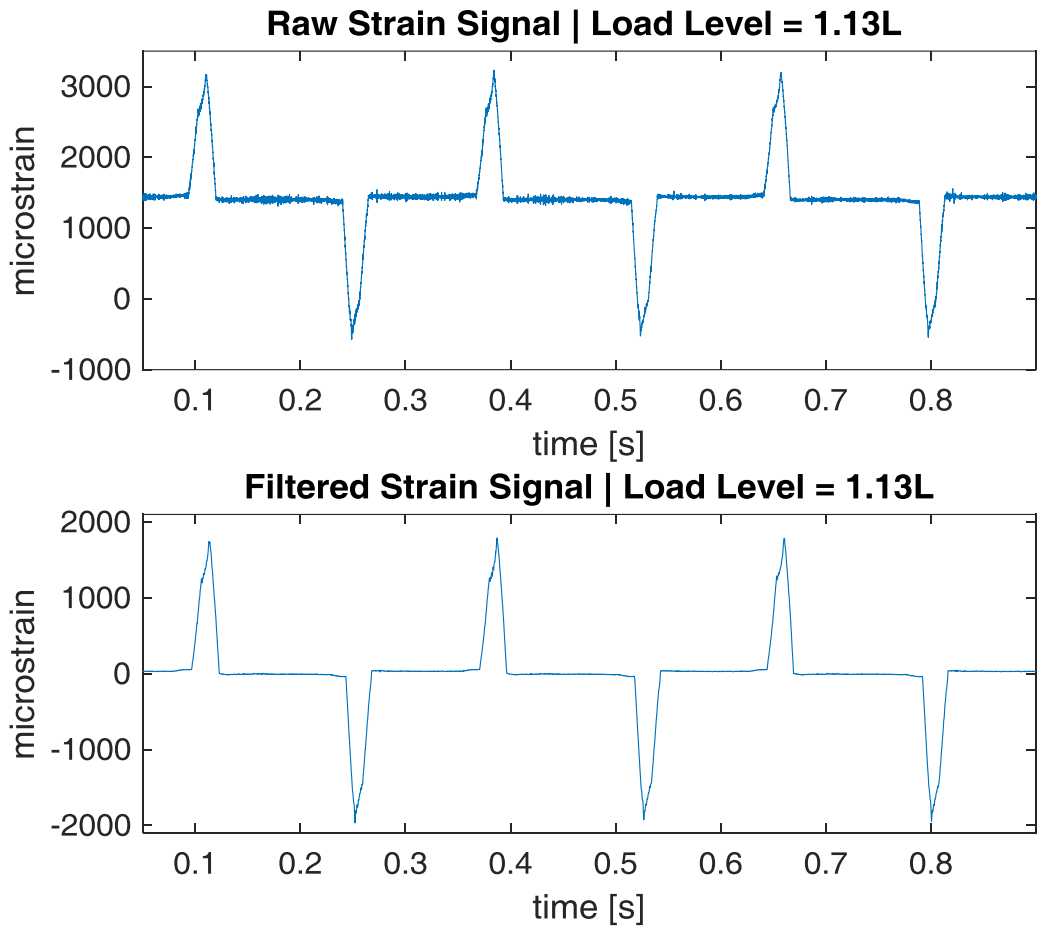

Figure 3.2: (a) Quasi-static strain time history sample for the load level 1.13*L*, and (b, c) the accompanying histograms of maximum compressive and tensile stresses.

Figure 3.2: Continued

(b)

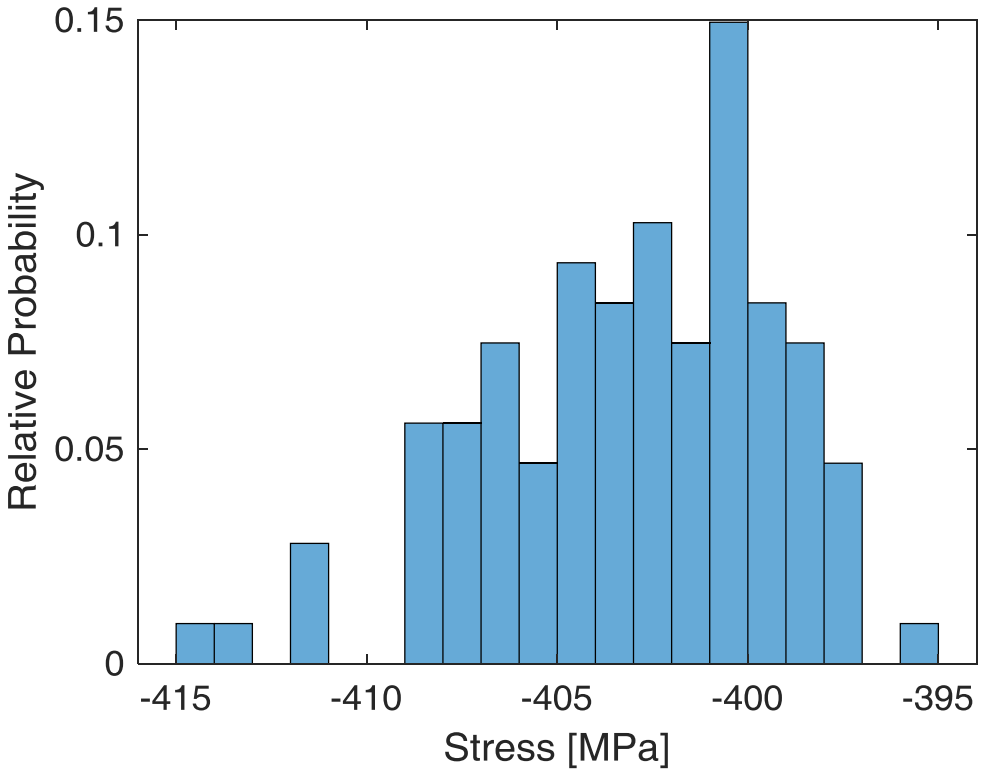

(c)

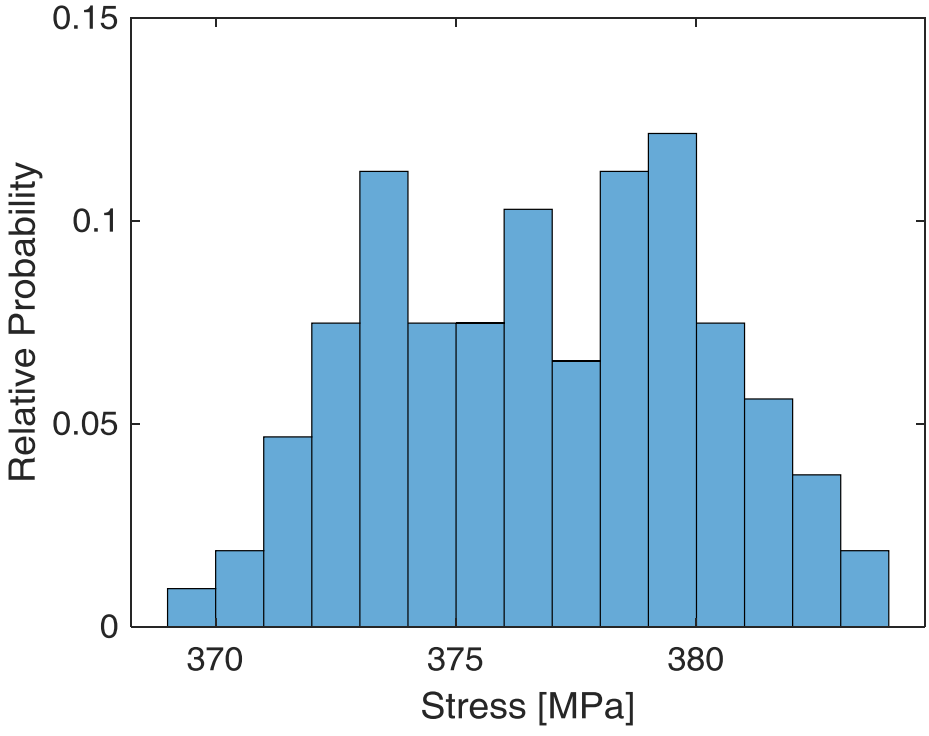

(a)

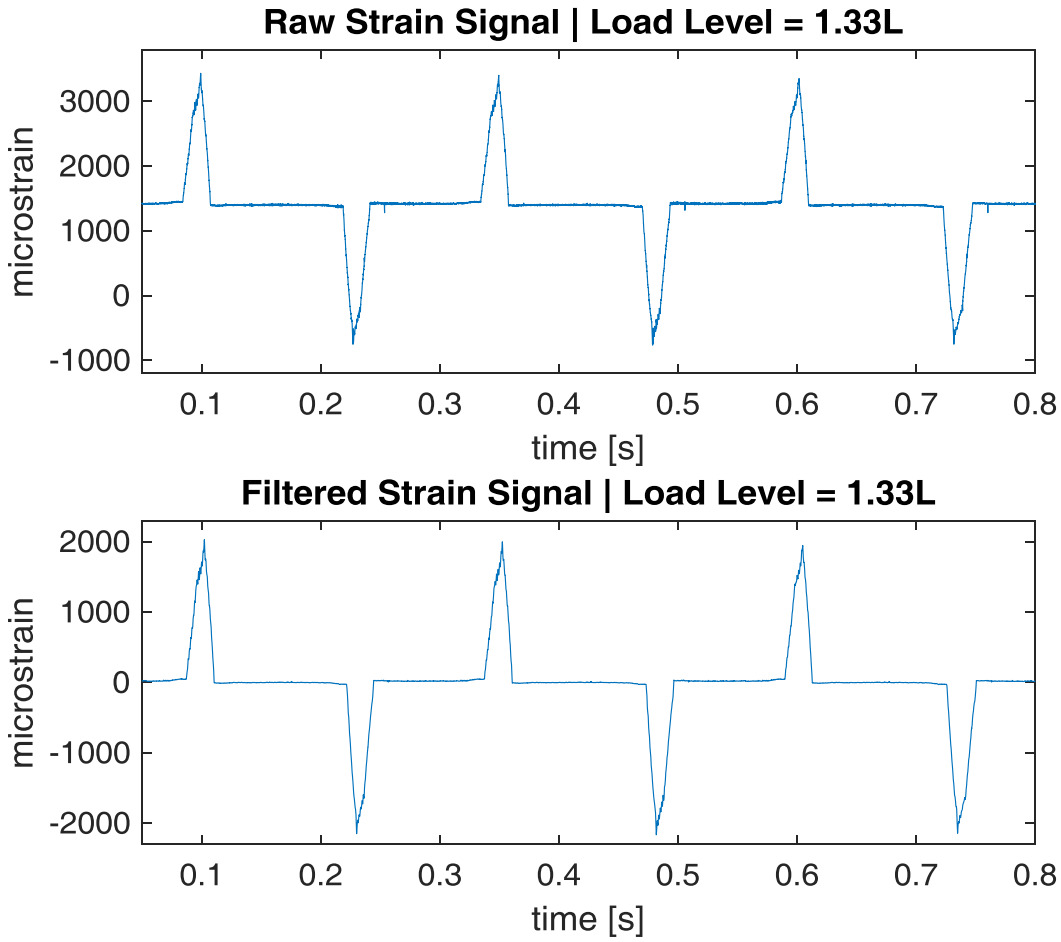

Figure 3.3: (a) Quasi-static strain time history sample for the load level 1.33*L*, and (b, c) the accompanying histograms of maximum compressive and tensile stresses.

Figure 3.3: Continued

(b)

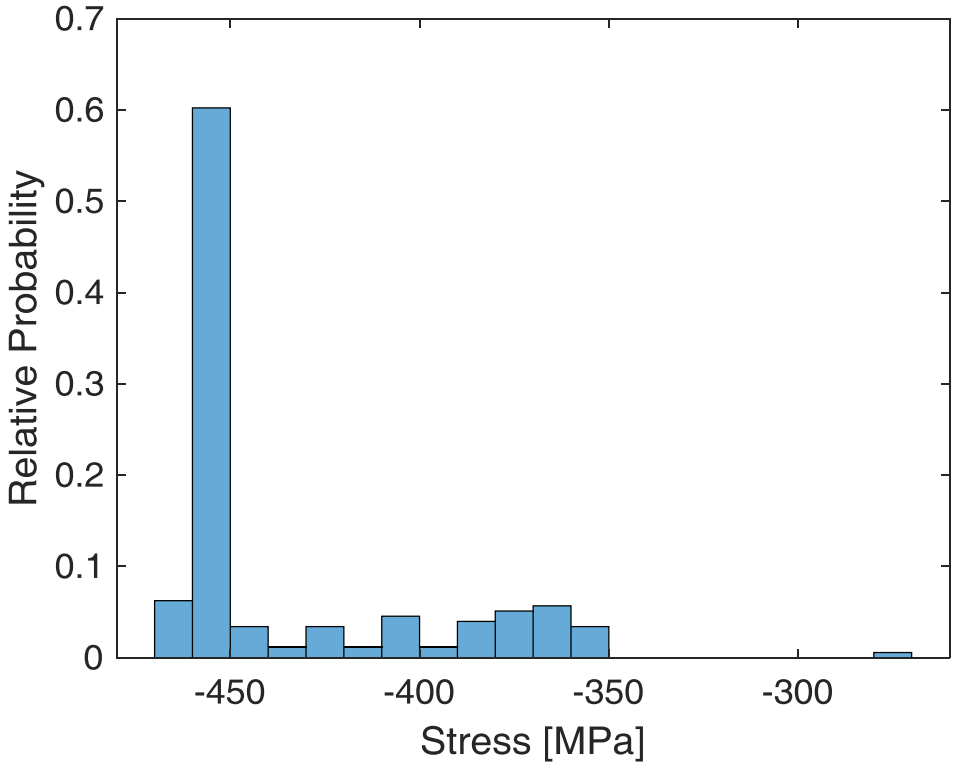

(c)

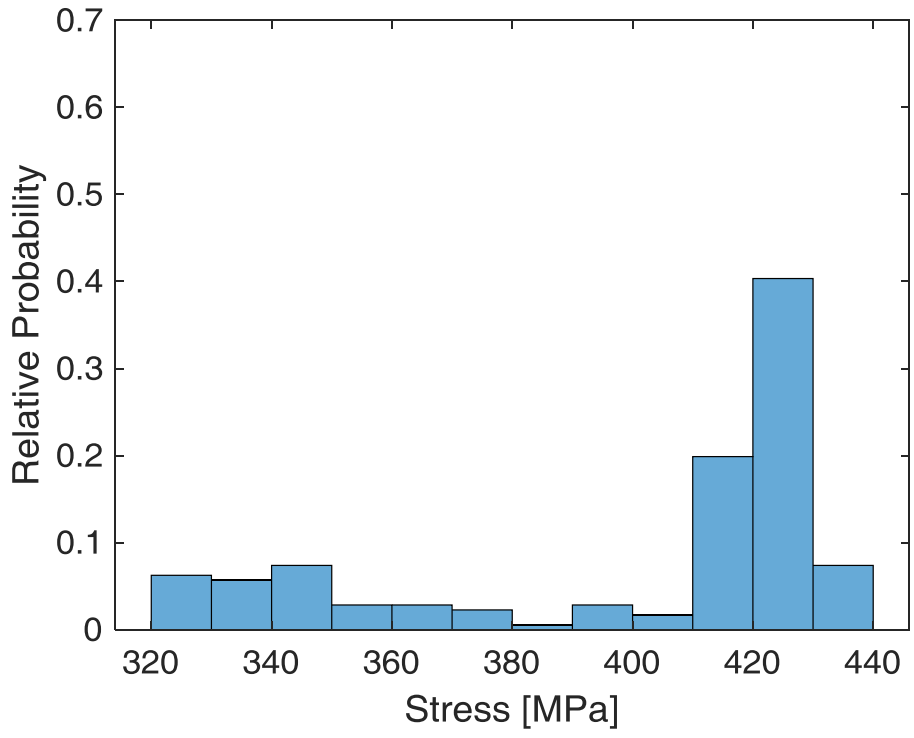

In this study, the pressure angle of the pinion ϕ = 26.842 degrees. As the pressure angle increases, radial forces on the gear tooth increase as well. The tangential force creates bending stress on either flank of the tooth, where the radial force creates an additional compressive force on the tooth of the gear. This results in a lower total tension force and a higher total compression force seen at the roots.

One last observation from the probability distributions of peak stresses is that the range in which the peaks fall in was quite narrow for each load. For instance, in Figure 3.1 (c), the range of tensile stress peaks was only 10 MPa, representing a $\pm 1.5\%$ band around the average peak stress of 306.1 MPa. This indicates that the quality of the test specimens as well as the test set-up were high enough to minimize scatter of the data.

3.3.2 Dynamic Test Results

Using the same methodology and presentation format of the previous section, strain time histories and the corresponding probability distributions of both compressive and tensile stress peaks are presented in this section for the dynamic speed condition of $\Omega_g = 3000$ rpm. Figure 3.4,Figure *3.5* andFigure *3.6* and show the measurements at load levels of *L*, 1.13*L* and 1.33*L*, respectively.

In Figure 3.4(a), raw strain signal exhibits some high frequency noise that was eliminated through proper filtering of the data, described in Section 3.2. In this filtered time history, the peak compressive and tensile strains were about 1750 and 1500 μstrain, respectively. Relative probability distributions shown in Figure 3.4(b, c) used 6453 data points (6453 revolutions of the pinion). As such, they are more detailed and show a

distribution representative of a normal distribution, suggesting that the data collected and experimental methods are valid. With the limited amount of peaks read in the quasi-static test runs, it was less apparent that the distribution of strain is normal as opposed to the dynamic test runs, which show clear normal distributions, save a few outliers. Despite this, none of the histograms suggests a multimodal distribution, which gives confidence in the measurements moving forward, as well as the calculations to find the average stress realized at the gage. The average peak stresses in Figure 3.4(b, c) were calculated as $\sigma =$ 365.4 MPa (compressive) and 323.5 MPa (tensile).

Figure 3.5 andFigure *3.6* show similar behavior at 1.13L and 1.33L, respectively. Similar levels of noise are observed in measured strain signals. The average peak stresses at 1.13L were $\sigma = 440.1$ MPa (compressive) and 382.3 MPa (tensile). The corresponding stress values at 1.33L were $\sigma = 474.1$ MPa (compressive) and 406.2 MPa (tensile).

3.4 Dynamic Factors

After verification of the quality of the data for each test run, the average peak strains for each tensile and compressive cycle were found for both quasi-static and dynamic tests. Table 3.1 lists the dynamic factors for tensile and compressible peaks calculated using Eq. (1.1). It is seen here that the dynamic factor for compressive peaks range from 1.09 to 1.13, indicating a 9 to 13% increase in peak stresses due to dynamic effects. Dynamic factors on the tensile side, meanwhile, are within 1.01 and 1.06, up to a 6% increase due to

(a)

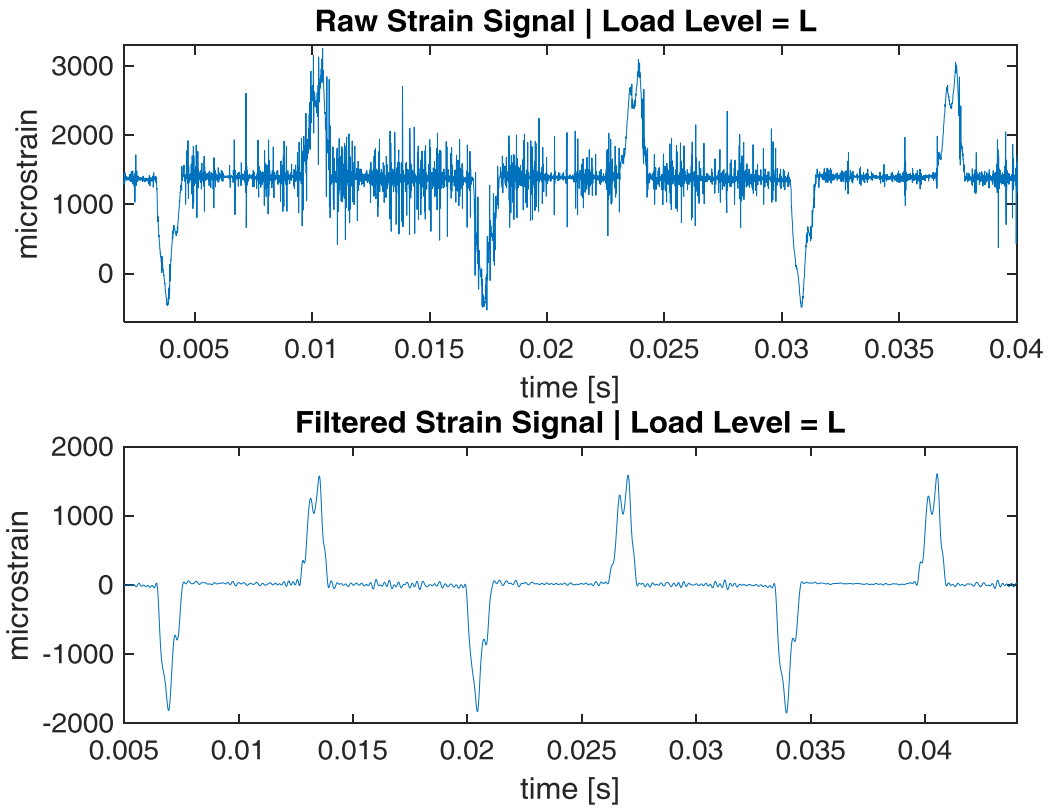

Figure 3.4: (a) Dynamic strain time history sample for the load level *L*, and (b, c) the accompanying histograms of maximum compressive and tensile stresses.

Figure 3.4: Continued

(b)

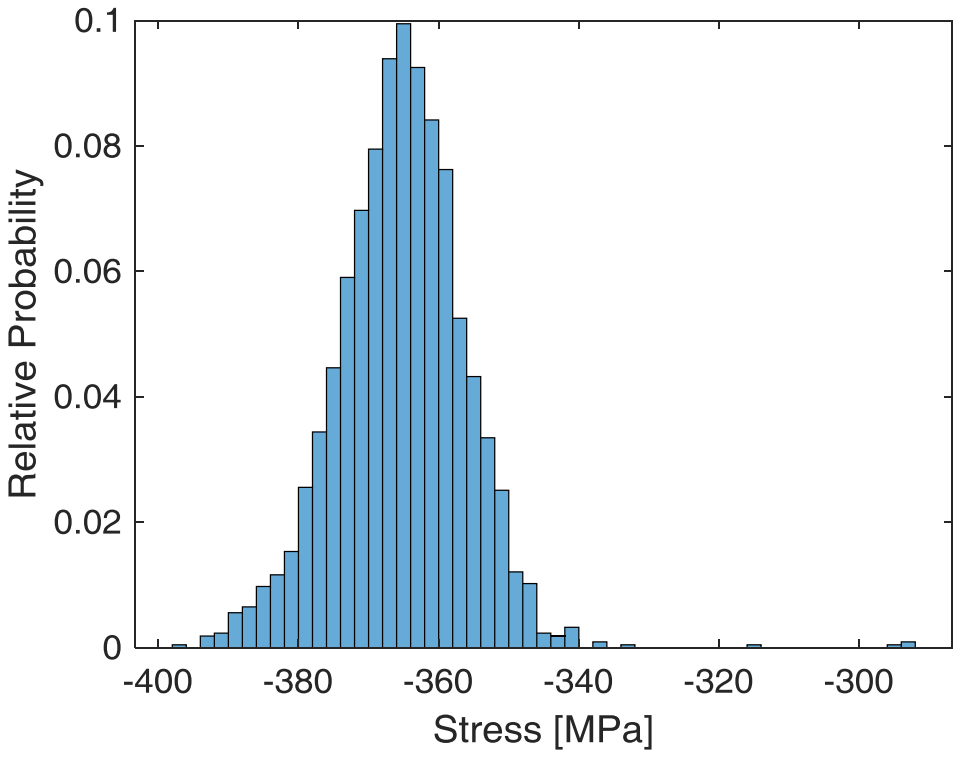

(c)

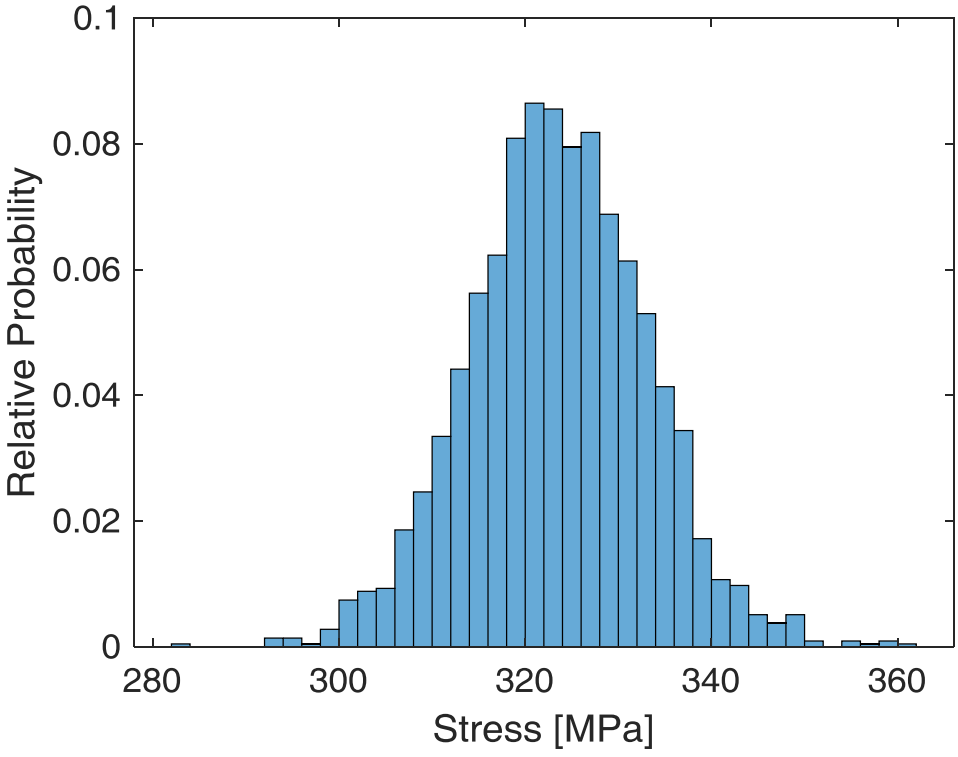

(a)

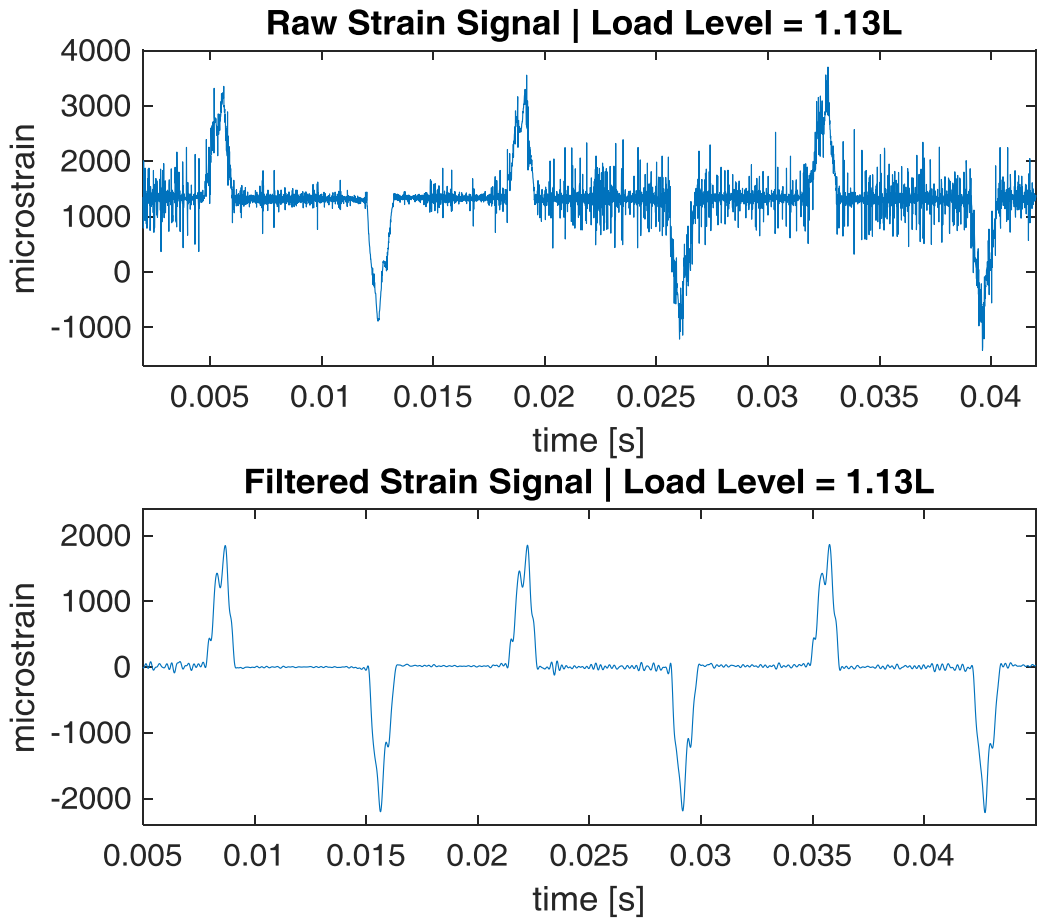

Figure 3.5: (a) Dynamic strain time history sample for the load level 1.13*L*, and (b, c) the accompanying histograms of maximum compressive and tensile stresses.

Figure 3.5: Continued

(b)

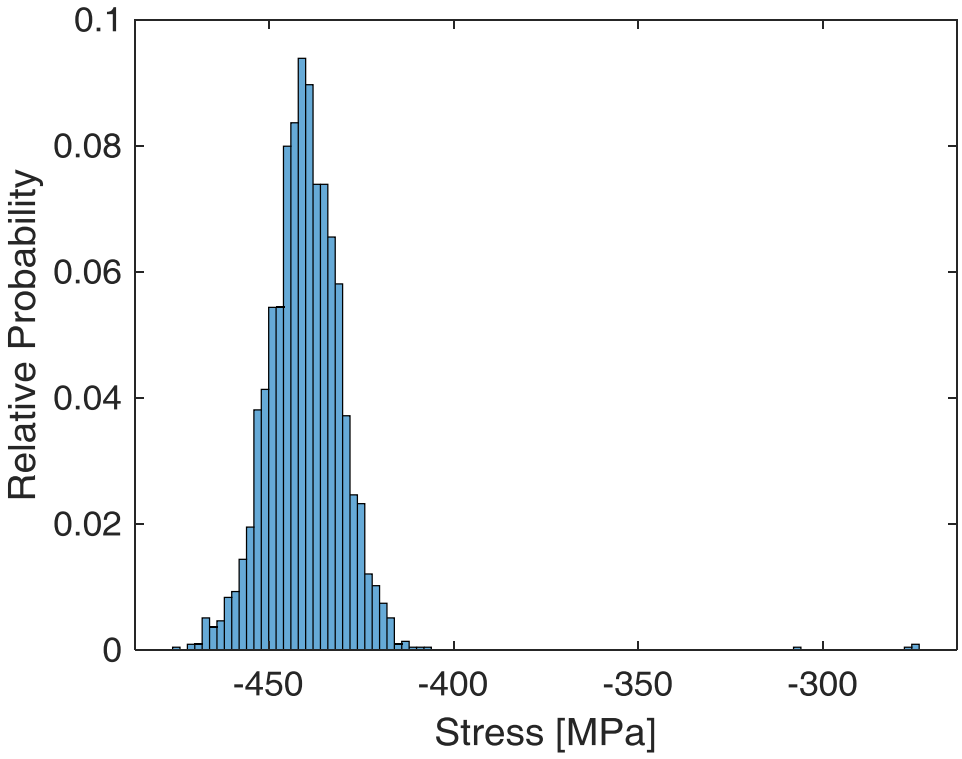

(c)

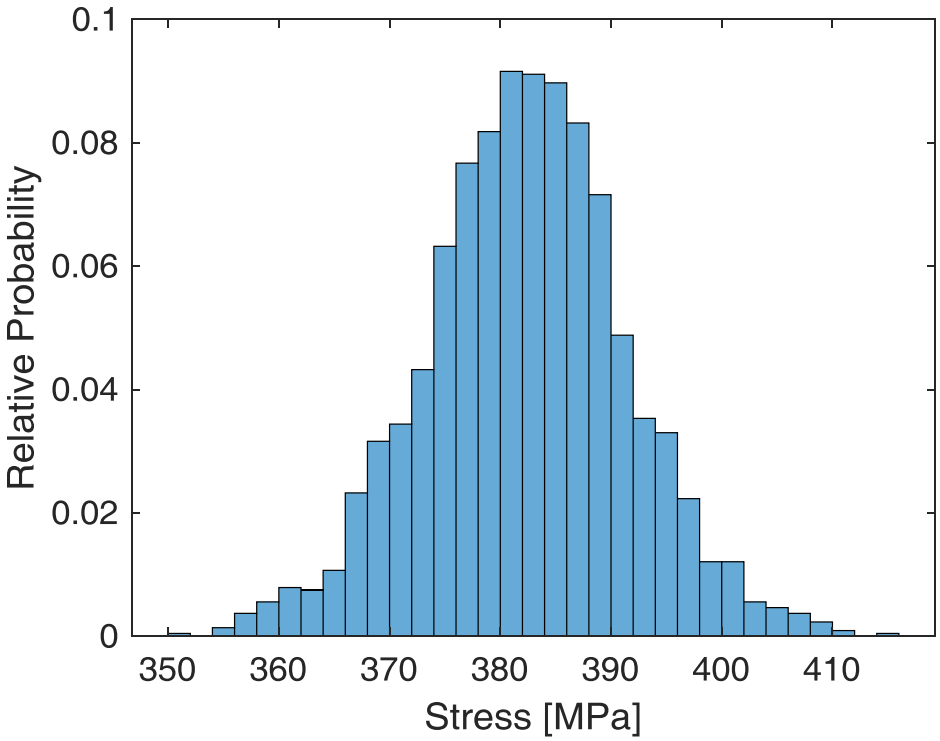

(a)

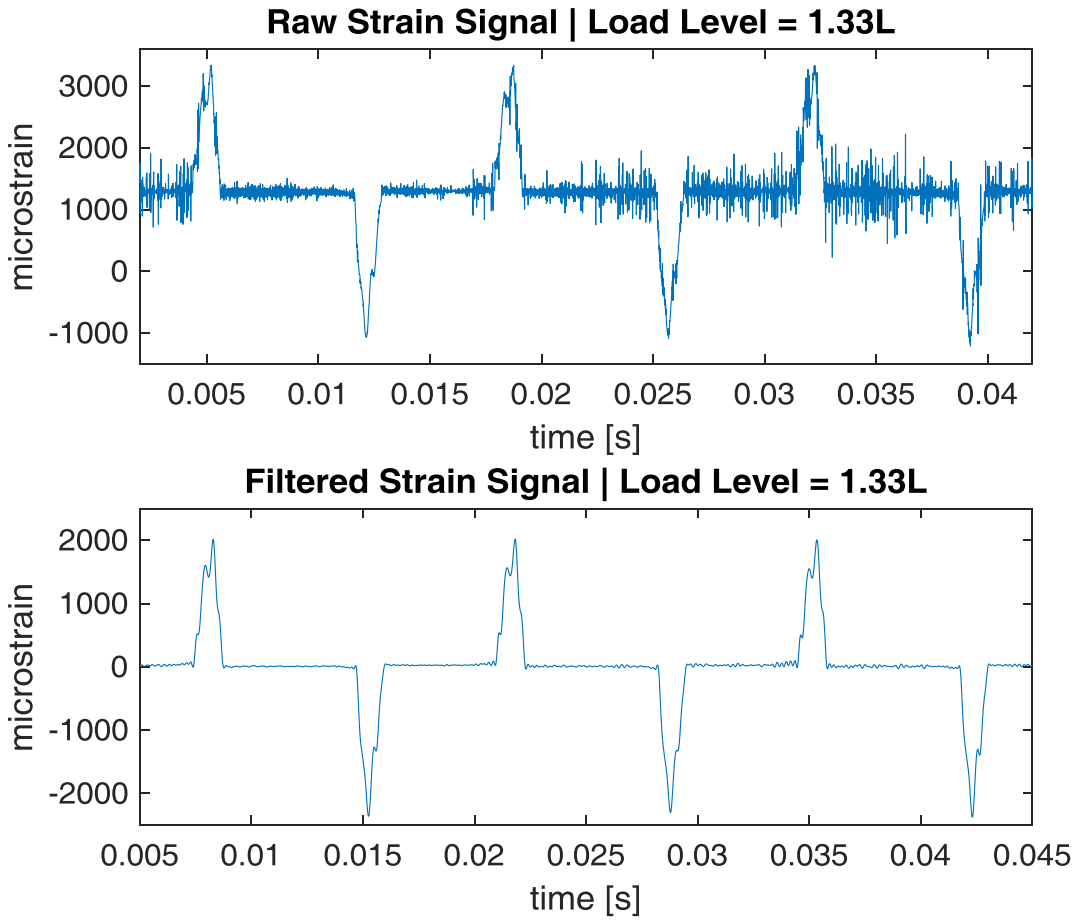

Figure 3.6: (a) Dynamic strain time history sample for the load level 1.33*L*, and (b, c) the accompanying histograms of maximum compressive and tensile stresses.

Figure 3.6: Continued

(b)

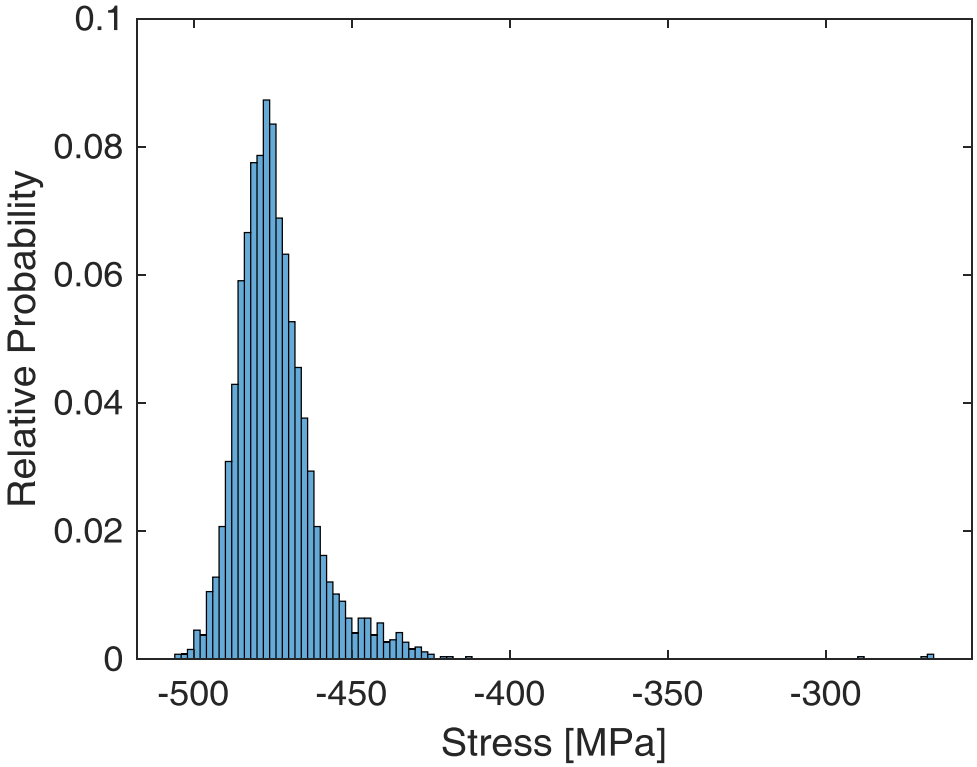

(c)

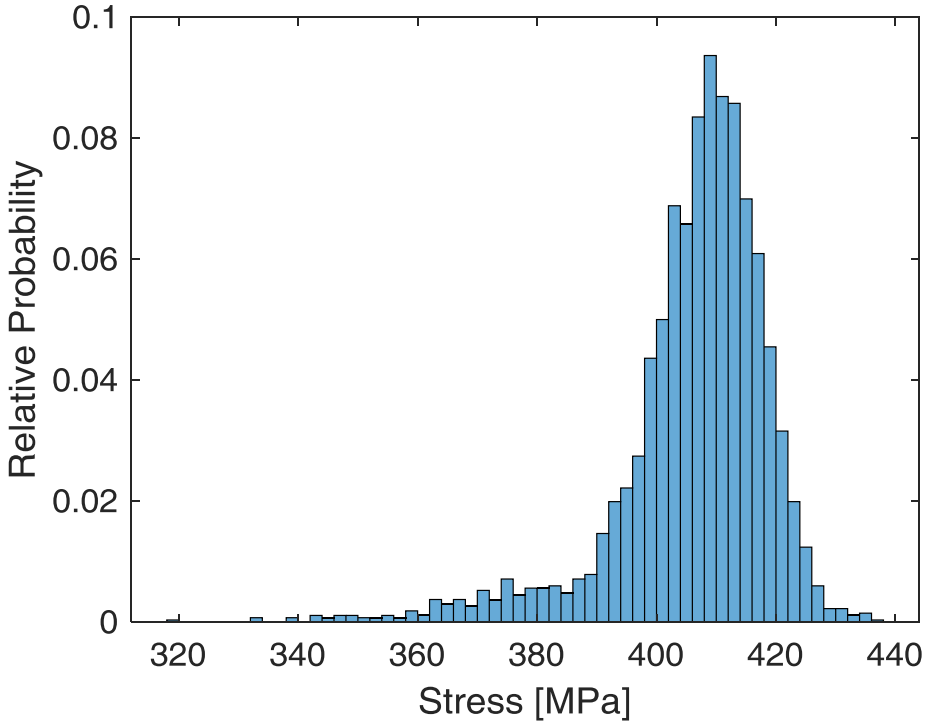

Table 3.1: Calculated dynamic factors at each load level for compressive and tensile sides of the test gear.

Load Level	DF	
	Tensile	Compressive
L	1.06	1.13
$1.13L$	1.01	1.09
$1.33L$	1.01	1.09

dynamic effects. These dynamic factor values can be applied to the corresponding static stresses in the resultant stress-bending life data to capture the dynamic influences of the test conditions.

The dynamic factors at the load levels listed in Table 3.1 can be viewed to be modest. Given the fact that the tests were performed at high-speed conditions where machine vibrations and resonances cannot be avoided, it can be still stated that speed of $\Omega_g = 3000$ rpm resulted in reasonably low dynamic factors. Even if they are modest, these dynamic factors should still be implemented in measured stress-life curves. Resultant fatigue damage *D* is proportional to the maximum stress σ according to $D \propto \sigma^n$ where exponent *n*, related to slope of the stress-life curve, is often between 7 and 9. With this, a 10% increase in σ would cause *D* to increase by $(1.1\sigma)^n$ representing $(1.1)^7$ to $(1.1)^9$ (or 1.95 to 2.35) times increase in *D*, which is rather significant.

Chapter 4

Conclusion

4.1 Summary

This study was aimed to quantify dynamic factors of a rotating spur gear within and high-speed gearbox. The main purpose was to develop and carry out a methodology to accurately and effectively measure root fillet strains of a test gear under both quasi-static and dynamic test conditions. By comparing data under these two conditions, a dynamic factor was determined under various torque conditions. This method of measurement will be employed and improved upon in future studies.

4.2 Major Conclusions

Using results discussed in the previous chapter, the following conclusions can be made about the study and its efficacy.

(i) The experimental methodology developed to measure gear dynamic factors based on root stress measurements was shown to be effective and accurate.

(ii) An idler gear was shown to have two different dynamic factors, one on the compressive side and the other on the tensile side.

(iii) The compressive side dynamic factors in this case were measured to be between 1.09 and 1.13, indicating that they must be included in the use of the fatigue data collected at this test speed value.

The methodology developed and demonstrated in this study will be employed in MS thesis research project aimed at comparing dynamic behavior of two separate machines designed to test the same test gear articles. As the methodology in this study was shown to be accurate and effective, it will form a stress-based assessment metric to complement other conventional means of vibration evaluations.

References

[1] Sun, A. "An Experimental Study of the Dynamic Response of Spur Gears Having Tooth Index Errors," M.S Thesis, The Ohio State University, Columbus, OH, 2015.

[2] Houser, D. R. and Seireg, A. “Evaluation of Dynamic Factors for Spur and Helical Gears,” *Transactions of ASME,* 504-514, 1970.

[3] Buckingham, E. “Dynamic Loads on Gear Teeth.” ASME Research Publication, New York, 1931.

[4] Harris, S. L. “Dynamic loads on the teeth of spur gears,” *Proc. Inst. Mech. Eng*., London, 87-112, 1958.

[5] ANSI/AGMA. “Fundamental Rating Factors and Calculation Methods for Involute Spur and Helical Gear Teeth,” ANSI/AGMA 2001 – D04. 2004.

[6] Talbot, D., Sun, A., Kahraman, A., “Impact of Tooth Indexing Errors on Dynamic Factors of Spur Gears: Experiments and Model Simulation,” *Journal of Mechanical Design*, **138**, 093302, 2016.

[7] Talbot, D., Kahraman, A., “A Dynamic Gear Load Distribution Model,” VDI International Gear Conference, Munich, Germany, October, 2015.

[8] Hotait, M.A., Kahraman, A., “Experiments on the Relationship between the Dynamic Transmission Error and the Dynamic Stress Factor of Spur Gear Pairs,” *Mechanism and Machine Theory,* **70**, 116-128, 2013.

[9] Tamminnana, V. K., Kahraman, A., Vijayakar, S. “On the Relationship between the Dynamic Factors and Dynamic Transmission Error of Spur Gear Pairs,” *Journal of Mechanical Design*, **129**, 75-84, 2007.

[10] Xu, H., Singh, A., Maddock, D., Kahraman, A., Hurley, J., "Thermal Mapping of an Automotive Rear Drive Axle," *SAE International Journal of Engines,* **4** (1), 888-901, 2011.

[11] Hong, I. “Impact of the Fully Reversed Loading Condition on Gear Tooth Bending Strength,” Ph.D. Dissertation Proposal, The Ohio State University, Columbus, OH, 2014.

[12] Kwon, H. S., Kahraman, A., Lee, H. K., Suh, H. S, “An Automated Design Search for Single and Double-Planet Planetary Gear Sets,” *Journal of Mechanical Design*, **136**, 061004, 2014.